

Design of efficient single-stage chirped pulse difference frequency generation at 7 μm , driven by a dual wavelength Ti:sapphire laser

Christian Erny · Christoph P. Hauri

Received: 19 December 2013 / Accepted: 13 April 2014 / Published online: 30 April 2014
© The Author(s) 2014. This article is published with open access at Springerlink.com

Abstract We present simulations for a design of a high-energy single-stage mid-IR difference frequency generation adapted to a two-color Ti:sapphire amplifier system. The optimized mixing process is based on chirped pulse difference frequency generation (CP-DFG), allowing for a higher conversion efficiency and reduced two-photon absorption losses. The numerical start-to-end simulations include stretching, chirped pulse difference frequency generation and pulse compression. Realistic design parameters for commercially available nonlinear crystals (GaSe, AgGaS₂, LiInSe₂, LiGaSe₂) are considered. Compared with conventional unchirped DFG directly pumped by Ti:sapphire technology, we predict a threefold increase in the quantum efficiency. Our CP-DFG scheme provides up to 340 μJ pulse energy directly at 7.2 μm when pumped with 8 mJ and supports a bandwidth of up to 350 nm. The resulting 240 fs mid-IR pulses are inherently phase stable.

1 Introduction

Intense laser pulses, tunable in the mid-infrared wavelength range (3–20 μm), are interesting for numerous applications, ranging from investigations of the fingerprint spectral region and semiconductors [1, 2] to the scaling of high-

order harmonic generation toward the water window and beyond [3–5]. A prominent approach for accessing this wavelength range is based on a multistage white-light seeded optical parametric amplifier (OPA) system, driven by a femtosecond Ti:sapphire laser system. While such BBO-based OPA stages typically provide tunable output between 1.3 and 2.6 μm , the longer wavelength range (3–20 μm) is typically accessed by an additional difference frequency generation (DFG) stage [6–8]. For such tunable systems, the typical conversion efficiency between the near-IR and the IR is rather small ($\approx 1\%$), with a corresponding quantum efficiency (QE) of $\approx 10\%$. The energy stability is limited by the multiple nonlinear conversion stages and the pulses are not intrinsically CEP stable for signal and idler mixing.

In the past, several DFG approaches based on AgGaS₂ (AGS) and GaSe (GS) have been presented. Throughout those efforts transform-limited (TL) or unchirped femtosecond pulses were used. Due to the high intensities and the subsequently strong TPA, only a low DFG efficiency could be achieved, which limited the generated output power significantly. Even though the applied laser systems provided pulse energies at 800 nm comparable to our system, the generated output energy between 7 and 10 μm was not exceeding 8 μJ with AGS [9, 10], corresponding to a pump to idler QE of 3.7%. In GS, up to 0.6 μJ has been produced between 10 and 20 μm (QE = 3.4%) [11].

In this paper, we present a different approach based on a single-stage, high-energy difference frequency generation, using chirped phase matching [12] between two intense laser pulses with different colors from a common Ti:sapphire amplifier source (Fig. 1).

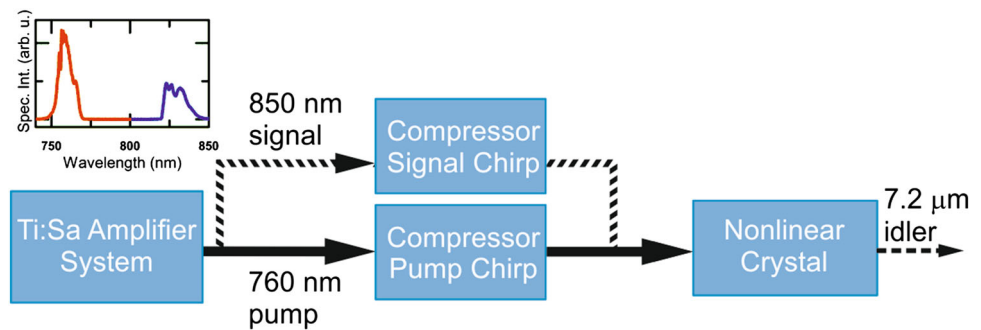
The scheme offers several advantages over DFG by unchirped pulses and the above-mentioned multistage OPA approach. It has the potential to provide increased energy

C. Erny (✉) · C. P. Hauri
Paul Scherrer Institute (PSI), SwissFEL, 5232 Villigen,
Switzerland
e-mail: christian.erny@psi.ch

C. P. Hauri
e-mail: christoph.hauri@psi.ch

C. Erny · C. P. Hauri
Ecole Polytechnique Federale de Lausanne, 1015 Lausanne,
Switzerland

Fig. 1 CP-DFG mixing scheme for dual-color Ti:sapphire laser amplifier system. Splitting and recombination of signal and pump are done by dielectric band-pass mirrors



stability, a simpler experimental setup, directly carrier envelope phase (CEP) stable [13, 14] mid-IR output pulses, an increased phase-matching bandwidth, as well as an increased interaction length and thus higher conversion efficiency. In particular, the chirped input pulses significantly reduce the impact of two-photon absorption (TPA) due to lower input intensity compared with the unchirped case.

Our investigation is motivated by recent progress in Ti:sapphire amplifier technology which is now capable to deliver synchronously a pair of intense pulses, which are easily tunable around their central wavelengths [15]. Thanks to the advancement of intra-cavity acousto-optic pulse shaping [16] in the regenerative amplifier, tunable two and more color operation up to 20 mJ at 100 Hz repetition rate has been demonstrated by our group [15]. The large wavelength separation (up to 90 nm) between the two pulses makes this source well suited for a single-stage direct DFG offering to cover a spectral range between 7 and 30 μm . The two colors can be separated by a suitable spectral beam splitter and sent into individual compressors. The polarization of the pump beam is controlled after the compressors. And the two chirped pulses are then recombined with a second mirror.

To our best knowledge, DFG with chirped input pulses from a Ti:sapphire laser has not been investigated up to present. DFG with chirped pulses offers the potential for significantly reduced TPA effect and offers thus higher output energies. We performed start-to-end simulations for chirped pulse difference frequency generation (CP-DFG) under realistic conditions, based on the above-mentioned two-color Ti:sapphire laser system. This includes chirping, nonlinear wave mixing, including two-photon absorption and subsequent pulse compression. The principal goal was to find the pump power, the amount of chirp, the crystal thickness, the beam size, and the compression scheme for broadband and efficient DFG. We predict that by CP-DFG a quantum efficiency of up to 60 % can be achieved while maintaining a large bandwidth. This exceeds largely the quantum efficiency of previous experimental implementations and of the conventional multistage OPA approach.

We show that the generated pulses can be compressed close to the transform limit by direct bulk material compressing.

We have structured this paper the following way. In the first part (Sect. 2), we discuss the simulation procedure necessary to optimize the parameter set and give an overview of the required nonlinear crystals. In the following sections, we make a comparison of the performance of DFG by transform-limited pulses (TL-DFG) and chirped pulses (CP-DFG) and demonstrate the expected performance improvement. Later we give an example for a realistic experimental realization (Sect. 5), including a simple compression scheme, based on bulk Germanium (Sect. 6). In the last section (Sect. 7), we give insight in the mixing process and we discuss the effects allowing CP-DFG to be three times more efficient than TL-DFG, showing that only a minor part of the improvement is related to the reduced losses. The major part comes from the fact that we can design the input beam parameters such that more photons are contributing to the mixing process and that the gain can be tailored such that the input photons are converted to the mid-infrared before they are absorbed by TPA.

2 Simulation and optimization

In recent years, many new materials have been developed for the application in the mid-IR wavelength range. Some of them have even been used for nonlinear mixing schemes [17], but most of them are still under development. For our wavelength mixing scheme suitable are the nonlinear materials AgGaS_2 (AGS), GaSe (GS), LiInSe_2 (LISE), and LiGaSe_2 (LGSe) [18]. AGS and GS are well established, but show high TPA. LISe and LGSe have a significantly smaller TPA coefficient, but also a lower nonlinear coefficient. All four materials have reasonably low absorption at 800 nm as well as at 7.2 μm and above (Table 1). To our best knowledge, these are the only nonlinear materials currently commercially available and suitable for our mixing scheme.

Table 1 Main properties of nonlinear crystal for DFG between 760 nm (pump) and 850 (signal) to 7.2 μm (idler)

	GS	AGS	LlSe	LGSe
Point group	6̄2 m	4̄2 m	mm ²	mm ²
Type (idler + signal → pump)	oo → e	oo → e	eo → e	eo → e
Plane	–	–	xy	xy
θ, φ phase-matching angle (°)	20.6	51.4	49.9	42.4
d _{eff} /(pm/V)	50.45	13.5	11.9	8
Nonlinear coupling constant κ (pm/V) ² /μm ²	25.2	1.5	1.6	1.3
Phase-matching bandwidth (nm)/(THz)	359/2.09	358/2.08	205/1.19	181/1.05
Two-photon absorption β (cm/GW)	6 [28]	4 [29]	0.6 [30]	<0.07 [30]
Transparency (μm)	0.62–20* [31]	0.48–11.4† [32]	0.72–10.4† [33]	0.37–13.2‡ [34]
700–900 nm absorption coefficient (cm ⁻¹)	<0.3 [35]	0.01 [35]	n. a.	n. a.
Idler absorption coefficient (cm ⁻¹)	<0.07 [35]	<0.04 [36]	n. a.	n. a.

Phase-matching type and plane have been chosen to maximize d_{eff} and bandwidth. The nonlinear coupling constant is given by κ² = d_{eff}²/(n₁n₂n₃λ₁λ₂λ₃). The transparency range is given at † α = 1cm⁻¹, ‡ α = 5cm⁻¹, and * “0” transmittance level

The main mixing parameters for the four nonlinear crystals are summarized in Table 1. For our studies, we have selected the phase-matching type providing the highest d_{eff} and bandwidth. We did only take into account collinear phase matching in the crystallographic planes.

As driving source for our DFG mixing, a dual wavelength Ti:sapphire laser system is considered, operating at 760 nm (pump, TL 53 fs) and 850 nm (signal, TL 66 fs) (Fig. 1), with a full width at half maximum (FWHM) bandwidth of 16 nm for both pulses and a repetition rate of 100 Hz. We are assuming Gaussian input pulses. The given maximum wavelength separation of 90 nm allows generating mid-IR radiation at 7.2 μm (idler). By reducing the wavelength separation between pump and signal, the idler could be tuned to longer wavelengths, but this is not the subject of this paper. Compared with the simulated QE for the presented mixing scheme, we expect the QE to scale with the coupling coefficient κ = d_{eff}²/(n₁n₂n₃λ₁λ₂λ₃) [19].

All simulations in this paper have been performed with a nonlinear propagation code by Arisholm [20]. The same code has been used successfully to model optical nonlinear interaction, e.g., optical parametric chirped pulse amplifiers (OPCPA [21]) at 800 nm [22] and 3.5 μm [23]. It numerically solves the equations for second-order nonlinear frequency mixing of full three-dimensional beams in an arbitrary birefringent crystal and takes into account the effects of depletion, diffraction, walk-off, and TPA.

For a given nonlinear crystal, the presented optimization problem is multidimensional, where both, the nonlinear gain and the TPA losses are driven by the total input intensity of pump and signal. Thus, the aim of our simulation was to find for each total input intensity pump chirp, ratio between pump and signal chirp, crystal length, and pump and signal energy. In a crystal, when TPA is not taken into account, the damage threshold and available

seed energy define the mixing conditions. In our case, we are not limited by the signal energy, but little is known about the damage threshold. Our calculations are thus covering the intensity range where we expect the damage limit. To take into account that any parameter modification might have an impact on the other parameters, we have applied the procedure as illustrated by Fig. 2.

This has been done through 1D simulations in the plane-wave approximation. For comparison, we have set the 1/e² beam radius for pump and signal to 5 mm for all crystals, all though LGSe is currently only available with 5 mm diameter. Diffraction effects on the mixing process can thus be neglected.

To reduce the parameter space, we have set initially the chirp ratio between pump and signal to a fixed factor according to chirp-assisted group-velocity matching [12]. The largest bandwidth in the TPA free case is expected for the following pump to signal chirp ratio:

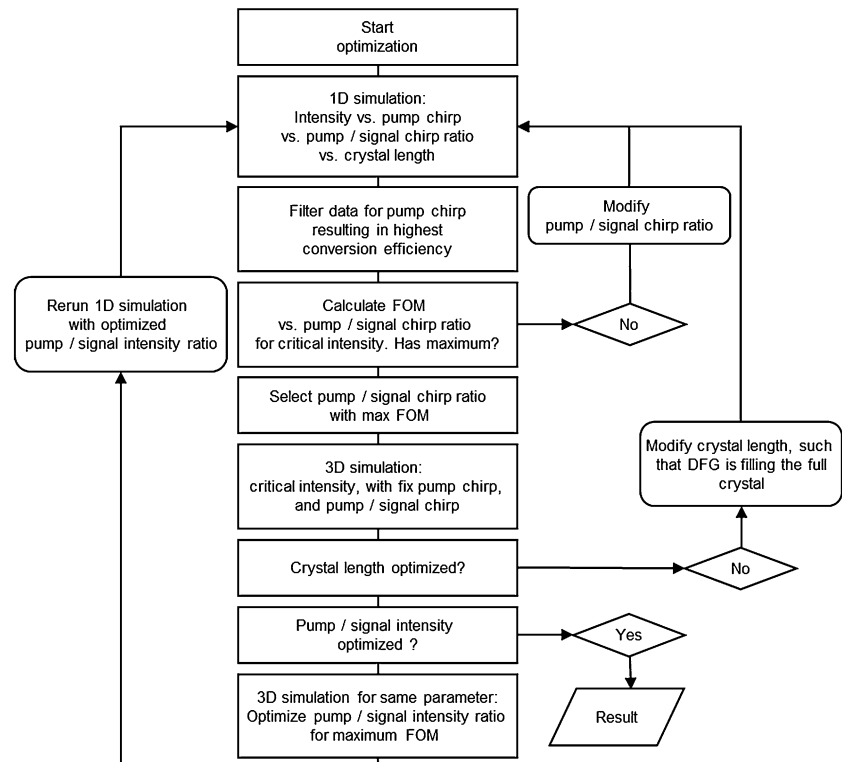
$$A_1 = 1 - \frac{n_{g,pump} - n_{g,signal}}{n_{g,idler} - n_{g,signal}} = \frac{GDD_{pump}}{GDD_{signal}}, \tag{1}$$

where GDD is the Group Delay Dispersion and n_g is the group-velocity index. The chirp ratio A₂ between signal and idler is then given by

$$A_2 = 1 - A_1 = \frac{GDD_{signal}}{GDD_{idler}}. \tag{2}$$

As TPA is depending on the spectral intensity, in the stretched pulse case, it appears as an additional spectral loss component, thus competing with the gain through phase matching. We therefore had to retrieve the optimized value for A₁ from our simulation. There is no longer a single chirp ratio that gives the best performance over the whole intensity range. We have therefore defined the following figure of merit (FOM)

Fig. 2 Flowchart of multidimensional optimization procedure



$$\text{FOM} = \frac{E \cdot \Delta\lambda}{I}. \quad (3)$$

This value depends on the idler pulse energy (E), its spectral FWHM bandwidth ($\Delta\lambda$), and the total pump and signal intensity (I). For further optimization, FOM is evaluated at a fixed intensity. Normally, the damage threshold would be a reasonable choice, but since it is unknown, we have defined a critical intensity based on the assumption that energy dissipation through TPA is the dominating limiting effect. Since only little data on the subject are available, we have based our definition on the earlier experimental implementation of DFG by compressed pulses by Xia et al. [13]. We have estimated in their experiment a 75 % loss of input energy in AGS due to TPA, an absorbed fluence of $\approx 3.8 \text{ mJ/cm}^2$, without damage in the crystal.¹

Based on their observation, we have defined the critical intensity where the loss fluence is 3.8 mJ/cm^2 for all investigated materials. Compared with the value from chirp-assisted group-velocity matching [12], the FOM optimum chirp factor is pushed to a higher value due to TPA (Table 2). Besides of this, the pump and signal pulses have the same sign in chirp, while the generated idler has the

¹ We have verified this experimentally for GaSe. By focusing a 4 mJ, 50 fs laser beam to 3.3 mm beam radius onto a 1 mm thick GaSe sample we measured an absorption of 3.3 mJ and a heating of the sample of 6 °C. We could not observe any damage.

Table 2 Parameter for optimum CP-DFG estimated from simulation

Material	Crystal length (mm)	Optimum chirp factor	Chirp factor from GVM	Intensity ratio signal/pump	Figure of merit
GS	1	1.35	1.25	0.48	12.8
AGS	2	1.30	1.25	0.82	13.7
LlSe	3	1.17	1.17	0.38	14.7
LGSe	2	1.35	1.13	0.29	6.5

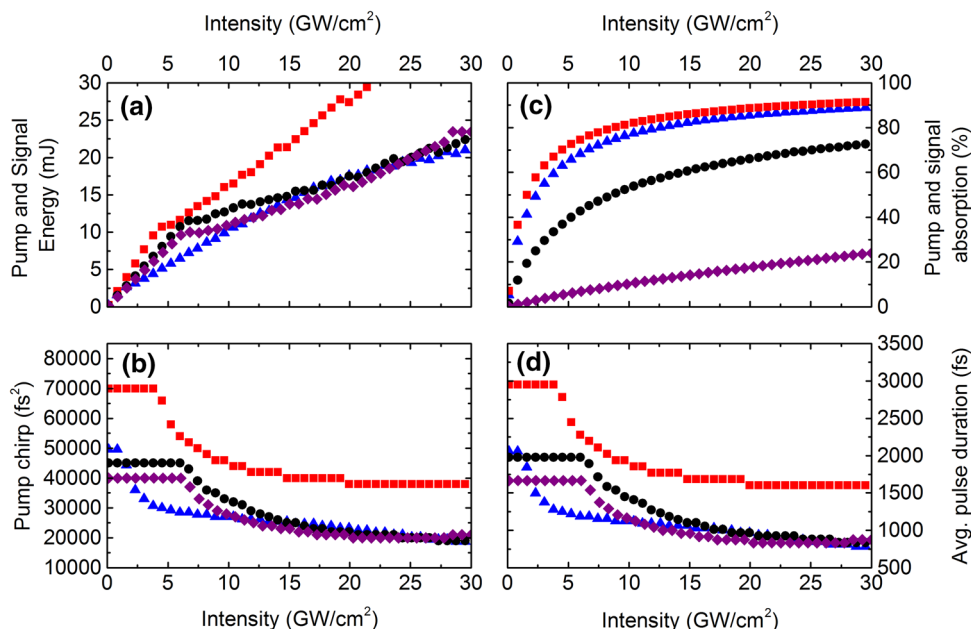
opposite chirp. In this article, we are only treating the case of positively chirped pump and signal, since the negatively chirped idler can be compressed by bulk materials.

To restrict the parameter range, we limited the maximum pump chirp to ≤ 3 ps depending on the nonlinear crystal considered (Fig. 3d). Typical pulse durations for the high intensities are between 1 and 2 ps. For lower intensities, the curves become divergent. The introduced chirp limitation prevents this asymptotic behavior.

On the basis of the above-found parameter sets for the critical intensity, the crystal length has been optimized through 3D simulations for no back conversions and then used for the second loop. In a final step, we have performed a pump to signal intensity ratio optimization for maximum FOM.

We also considered a strong contribution from the cross-TPA terms originating from the absorption of the signal

Fig. 3 Parameter set for optimized CP-DFG (a) and (b) in dependence of the total (pump and signal) intensity. **a** Total required input energy for a 10-mm-diameter nonlinear crystal for GS (blue triangles), AGS (red squares), LIGe (black dots), and LGSe (purple diamonds), **b** required pump chirp value for maximum output energy, **c** resulting total input absorption, and **d** average input pulse duration. The chirp of the signal is related to the pump chirp by the chirp factor from Table 2



induced by an intense pump and vice versa. Unfortunately, little is known about these coefficients, but as a reasonable upper limit approximation, we have taken the diagonal coefficient values, corrected by a factor of 2 to take the weak wave retardation into account [24].

Other parasitic processes (e.g., thermo optic effect and linear absorption) are neglected. We have estimated the impact of nonlinear refractive index based on data available for similar nonlinear materials. For example, for silicon waveguides [25] and AgGaSe₂ [26, 27], TPA coefficient and nonlinear refractive index are available. For both materials, the TPA coefficient is ranging between 1 and 10 cm/GW and the corresponding nonlinear refractive index 3×10^{-5} – 6×10^{-5} cm²/GW for 1.5 μm wavelength. We assumed similar values for GS and AGS. A nonlinear refractive index of up to 10×10^{-5} cm²/GW did not show a significant impact according to our simulations.

For each total (pump plus signal) input intensity, this resulted in a set of total input energy (Fig. 3a), pump chirp (Fig. 3b), pump to signal chirp factor, absorption (Fig. 3c), pump to signal intensity ratio, and crystal length (Table 2) for the optimized CP-DFG.

3 TL-DFG and its limitations

As a benchmark, we first calculated conventional DFG with TL pump and signal and for different DFG crystal types in dependence of the total input intensity. The calculation shows that even at high intensities up to 80 GW/cm² and with a total input energy of 4 mJ not more than 40 μJ output can be achieved at a wavelength of 7.2 μm (Fig. 4a). This is in-line with the reported results [9, 10]. In

TL-DFG, the main limiting factor for a larger conversion into the idler is the high loss through TPA and the group-velocity mismatch. This loss increases rapidly even at low intensities (i.e., a few GW/cm²) and surpass 80 % for intensities above 40 GW/cm² (LIGe, AGS, and GS) (Fig. 4b).

This large and detrimental impact of TPA in the mixing process can only be controlled by reducing the input intensity, which does not correct for the group-velocity mismatch in the TL case. However, CP-DFG can control both effects.

4 Chirped pulse DFG

We illustrate the potential of CP-DFG by presenting first the optimized achievements against the TL case (Fig. 5). By inducing the ideal chirp (Fig. 3) to both pump and signal, the output energy can be increased by an order of magnitude, while reducing the input intensity. The FWHM bandwidth is also enhanced by CP-DFG (Fig. 5c, d). It can be observed that the output energy scales linearly with the input intensity. The sharp edge around 5 GW/cm² is due to our chirp limitation. Here, significantly longer pump and idler pulses would be required to maintain the linear behavior. On the high-intensity side, GS shows a saturation behavior. The strong nonlinear coefficient leads to back conversion, which could be prevented by a shorter crystal.

The best performance in terms of conversion efficiency can thus be expected for the newer Li-based materials, while GS and AGS support larger gain bandwidth.

To get more realistic estimation for experimental implementation, we have performed the simulation for the

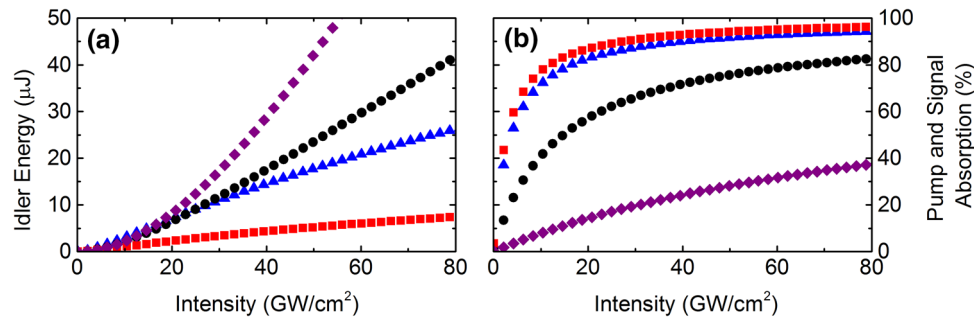
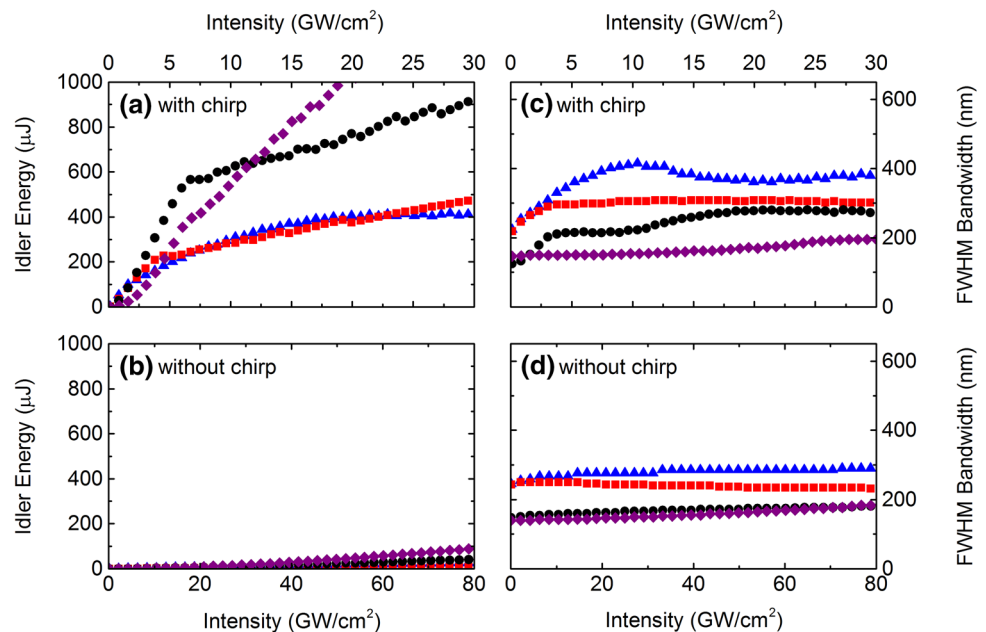


Fig. 4 Conventional DFG with transform-limited pulses. Achievable output power **(a)** and pump and signal absorption **b** for DFG with compressed pulses in 10-mm-diameter 2-mm-long AGS (*red*

squares), 1-mm-long GS (*blue triangles*), 3-mm-long LISe (*black dots*), and 2-mm-long LGSe (*purple diamonds*)

Fig. 5 Achievable output power and bandwidth for 10-mm-diameter AGS (*red squares*), GS (*blue triangles*), LISe (*black dots*), and LGSe (*purple diamonds*). **a** CP-DFG idler energy, **b** DFG energy achieved with compressed pulses with the corresponding FWHM bandwidth (**c**, **d**)



critical intensity in 3D. The values for pump chirp, chirp ratio, and pump to signal intensity ratio have been taken from the parameter scan from above. The results are summarized in Table 3.

With CP-DFG, the output power generated from AGS can reach up to $107 \mu\text{J}$, whereas in the unchirped case only $6 \mu\text{J}$ is possible. This value is similar to the experimental result from Xia et al. [9]. Although they used slightly different mixing conditions, the good agreement corroborates the validity of our model.

Even though AGS and GS exhibit extremely strong TPA, by the reduced intensity through the chirping of the pulses, we can achieve output energies of up to $163 \mu\text{J}$. With the given pump energy of 3.7 mJ , this corresponds to a quantum efficiency of 42% . In the unchirped case, one would expect from total 3.2 mJ pump and signal power to produce $21 \mu\text{J}$ in the mid-IR, thus a quantum efficiency of only 14% . For LISe and LGSe, the QE can be improved

from 14 to 50% and from 32 to 60% , respectively, by moving to the CP configuration.

The alternative approach to reduce the intensity and as a result the TPA is to increase the beam size. This, however, does not compensate for the group-velocity mismatch. In GS, we estimate an output energy of $20 \mu\text{J}$ for the same pump intensity as for CP-DFG and a beam radius of 20 mm from Fig. 4a), which gives the same output energy as with the smaller beam size.

5 Temporal pulse compression

The consequence of the CP-DFG approach is that the generated mid-IR pulse is strongly chirped. The large amount of dispersion needed to recompress the narrow-band mid-IR pulse (ca. 5% bandwidth) would require large prism or grating separation in the compressor, thus

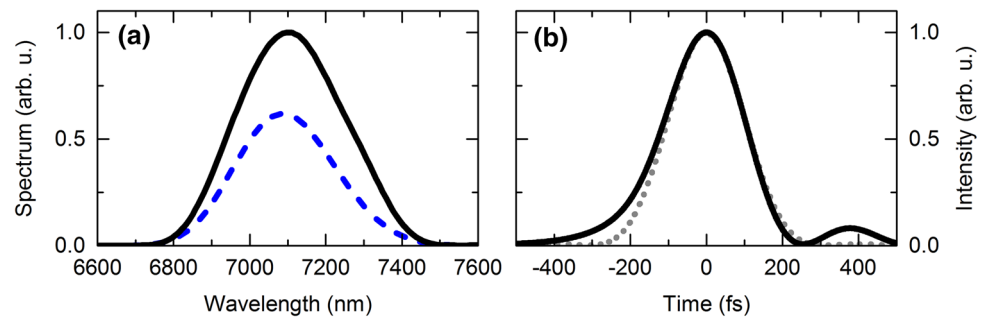
Table 3 3D simulation of maximum output power for GS, AGS, and LISe and highest bandwidth for LGSe

Material	Intensity (GW/cm ²)	Chirp 760 nm/850 nm (fs ²)	Pump energy 760 nm/850 nm (mJ)	Output energy (μJ)	Bandwidth (nm)	Bulk Ge for compression (mm)	Compressed pulse duration (fs)
1-mm GS	4.4	30750/22778	3.7/1.1	163	345	159	242
2-mm AGS	2.2	70000/53846	3.5/1.7	107	281	438	286
3-mm LISe	4.6	45000/38461	6.2/1.6	339	200	515	457
2- mm LGSe	20.7	20000/15384	3.3/0.6	211*	160	101	327

* Output energy for a $2 \times 5 \times 5$ mm LGSe crystal

Fig. 6 Compressed idler output from CP-DFG in 1-mm GS

a Spectral intensity at 0.4 mm inside the nonlinear crystal (Blue dashed line) and at the output. **b** Bandwidth limited (Gray dotted line) and compressed (Black solid line) pulse shape at the output after passing through 160-mm Ge



making this scheme unfeasible. Therefore, we propose recompression of the negatively chirped idler in bulk material. The amount of dispersion can be estimated from (2). A 200-mm-long Germanium rod can cover up to $-150'000$ fs² of chirp (GDD of 745 fs²/mm). The limitation of this compression scheme is that it does not allow for fine-tuning. To achieve maximum compression, one needs to accurately adjust the chirp prior to compression. This can be done by adjusting the chirp of the two IR pulses, while maintaining the chirp ratio. This scheme, however, does not allow controlling the third-order dispersion. Due to the residual third-order dispersion, the generated output pulse has a small pre-pulse. In the case of GS, where potentially the shortest pulses can be generated, the bandwidth-limited pulse duration is 232 fs. By bulk compression in 159-mm Germanium (Fig. 6a, b), 242 fs can be achieved.

6 Dynamics during generation

The simulations offer insight into the dynamics occurring during the mixing process and allocate where the additional idler energy is coming from. A large contribution comes from the fact that about 50 % more pump energy is available for CP-DFG mixing process. The critical intensity is between 5 and 10 GW/cm² for CP-DFG, whereas in the unchirped case, it exceeds 70 GW/cm². For GS, at the latter intensity, the TPA absorption exceeds 90 %, while at ~ 5 GW/cm², it is reduced to 60 % (Fig. 4b). Similar ratio is observed for the other nonlinear crystals (Fig. 4b). Since we fixed the loss density for this comparison, the pump

energy for CP-DFG can be a factor of 1.5 higher. This increases the possible output power without affecting the quantum efficiency. We can visualize the nonlinear wave mixing through our simulation by analyzing the spectra inside the nonlinear crystal during the mixing process. We have chosen GS since it shows the strongest coupling and TPA. First, we analyze the energy transfer to the mid-IR (Fig. 7a, d). In the case of unchirped input pulses, the mixing process is terminated after about 0.3 mm with 21 μJ output energy. The interaction length is limited here by group-velocity mismatch, while TPA mainly affects the output energy. With CP-DFG and equally intense input beams after about 0.4 mm back conversion would set in (Fig. 7d, dashed line). Normally, one would choose this as the crystal length, but due to strong TPA, a significant amount of the signal has been absorbed and is now too weak to drive strong back conversion. Effectively, this just reduces the idler gain. After a short distance, a second DFG step is taking place. By reducing the signal intensity while increasing the pump intensity, the gain can be controlled, such that point of back conversion can be shifted to the end of the nonlinear crystal and a smooth energy flow can be achieved. This way by modifying the chirp and the intensity ratio between the pump and the signal, we can optimize the process, such that the full crystal length can be used. This cannot be achieved by reducing the intensity of TL pulses. By this approach, we could improve the output energy from 127 to 167 μJ . While in the first case, for the equal pump and signal intensity, 2.7 mJ pump energy and 1.6 mJ signal energy are required, in the optimized case, 3.7 mJ pump energy and 1.1 mJ signal energy are

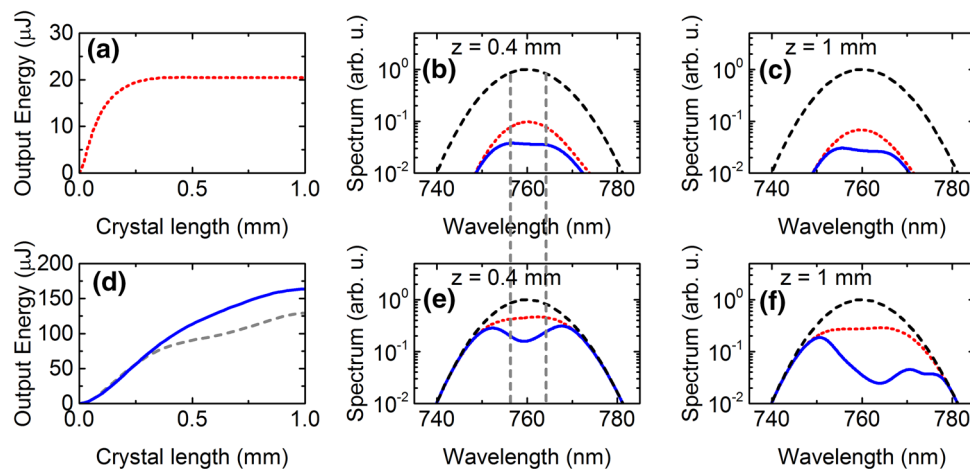


Fig. 7 Dynamics of mixing process for CP-DFG (**a–c**). **a, d** Idler power inside nonlinear crystal (GS) for compressed pump and signal (*blue solid line*: with intensity ratio optimization, *gray dashed line*: pump and signal with equal intensity). **d–f** Dynamics of CP-DFG

according to the values from Table 3. **b, c, e, f** pump spectra at input (*black dashed line*), at 0.4 and 1 mm, respectively, inside the crystal (*blue solid line*) and the impact of TPA only without nonlinear mixing (*red dotted line*)

necessary. Thus, the relevant number of photons for the mixing process could be improved by 35 %.

By looking at the pump spectrum inside the mixing crystal, one can see the nature of the mixing process (Fig. 7b, c, e, f). In the case of unchirped input pulses, we can observe that TPA affects all parts of the spectrum equally. Thus, the relatively weak spectral wings suffer a much higher loss through TPA than in the case of chirped phase matching. For the CP-DFG case, TPA leads to a flat-top like spectrum, whereas the shape of the spectrum is not modified for the unchirped inputs, but just reduced in intensity. The flat-top spectrum supports a larger FWHM bandwidth than the Gaussian spectrum. From the depletion of the spectra, one can identify the spectral parts that actually have taken part in the mixing process. In the unchirped case, this is 10 nm around the peak, compared with the 17 nm calculated for the chirped case. Assuming Gaussian pulses, there is about 35 % more energy available for the mixing process in the chirped case. Furthermore, a stronger depletion of the pump can be achieved, resulting in a higher conversion efficiency. Even though a larger part of the spectrum has already been used in the first part of the crystal, there is still between 25 and 30 % of the initial energy left in the spectral wings. Due to the strong pump depletion and chirp, this can be considered as a delayed fresh pump pulse at slightly longer wavelength, which continues driving the DFG interaction. The simulation reveals also how the interaction wavelength shifts from the short wavelength to the long wavelength as the pulses pass through the crystal. In the current configuration, this shift is mainly mapped to the signal to maintain phase-matching conditions, while the idler is only slightly shifted to longer wavelength (Fig. 6a).

Taking the small improvements from the reduced losses, the modified pump to signal intensity ratio, the larger interaction bandwidth, and the stronger pump depletion together, this results in a factor 3 higher quantum efficiency. The higher available input power at the same loss level results in a further enhanced output power of up to a factor of 8. In summary, the main contribution to the increased QE is that more photons of the pump pulse are taking part in the mixing process and that one can sequentially increase the pump energy and number of pump photons, without changing the losses and while maintaining the intensity. Thus, the optimized CP-DFG interaction results in an efficient energy transfer from the pump to idler. This means that the energy is transferred to the idler before it can be absorbed through TPA.

7 Conclusion

In conclusion, we have designed a chirped pulse DFG stage that has the capability to efficiently mix the direct output from a dual wavelength Ti:sapphire amplifier system to the mid-IR. We have shown that the conversion efficiency can be significantly improved by chirped wave mixing compared with conventional unchirped DFG. We could show that the higher efficiency is related to the fact that a significant higher number of photons are contributing to the interaction.

Based on different commercial available nonlinear crystals, the system is capable of delivering more than 340 μJ pulse energy and pulses as short as 242 fs at 7.2 μm central wavelength. The generated pulses are inherently CEP stable. The two-color tunability offered by the

Ti:sapphire system in combination with the investigated nonlinear material potentially allows the emission of up to 16 μm .

Acknowledgments We would like to acknowledge fruitful discussions with Gunnar Arisholm, as well as the financial support from SNSF (Grant No. PP00P2_128493). C.P.H. acknowledges association to NCCR-MUST.

Open Access This article is distributed under the terms of the Creative Commons Attribution License which permits any use, distribution, and reproduction in any medium, provided the original author(s) and the source are credited.

References

- W. Kuehn, K. Reimann, M. Woerner, T. Elsaesser, R. Hey, U. Schade, *Phys. Rev. Lett.* **107**, 067401 (2011)
- F. Junginger, B. Mayer, C. Schmidt, O. Schubert, S. Mährlein, A. Leitenstorfer, R. Huber, A. Pashkin, *Phys. Rev. Lett.* **109**, 147403 (2012)
- C.P. Hauri, R.B. Lopez-Martens, C.I. Blaga, K.D. Schultz, J. Cryan, R. Chirila, P. Colosimo, G. Doumy, A.M. March, C. Roedig, E. Sistrunk, J. Tate, J. Wheeler, L.F. DiMauro, E.P. Power, *Opt. Lett.* **32**, 868 (2007)
- T. Popmintchev, M.-C. Chen, D. Popmintchev, P. Arpin, S. Brown, S. Ališauskas, G. Andriukaitis, T. Balčiunas, O.D. Mücke, A. Pugzlys, A. Baltuška, B. Shim, S.E. Schrauth, A. Gaeta, C. Hernández-García, L. Plaja, A. Becker, A. Jaron-Becker, M.M. Murnane, H.C. Kapteyn, *Science* **336**, 1287 (2012)
- M.-C. Chen, C. Hernández-García, C. Mancuso, F. Dollar, B. Galloway, D. Popmintchev, P.-C. Huang, B. Walker, L. Plaja, A. Jaron-Becker, A. Becker, T. Popmintchev, M. M. Murnane, and H. C. Kapteyn, arXiv:1401.0240 [physics] (2013)
- F. Seifert, V. Petrov, M. Woerner, *Opt. Lett.* **19**, 2009 (1994)
- R.A. Kaindl, M. Wurm, K. Reimann, P. Hamm, A.M. Weiner, M. Woerner, *J. Opt. Soc. Am. B* **17**, 2086 (2000)
- A. Sell, R. Scheu, A. Leitenstorfer, R. Huber, *Appl. Phys. Lett.* **93**, 251107 (2008)
- J.F. Xia, J. Song, D. Strickland, *Opt. Commun.* **206**, 149 (2002)
- K. Yamakawa, C.P.J. Barty, *Opt. Lett.* **28**, 2402 (2003)
- J.M. Fraser, I.W. Cheung, F. Légaré, D.M. Villeneuve, J.P. Likforman, M. Joffre, P.B. Corkum, *Appl. Phys. B* **74**, s153 (2002)
- K. Osvey, I.N. Ross, *J. Opt. Soc. Am. B* **13**, 1431 (1996)
- H.R. Telle, G. Steinmeyer, A.E. Dunlop, J. Stenger, D.H. Sutter, U. Keller, *Appl. Phys. B* **69**, 327 (1999)
- Y. Deng, F. Lu, W. Knox, *Opt. Express* **13**, 4589 (2005)
- A. Trisorio, P.M. Paul, F. Ple, C. Ruchert, C. Vicario, C.P. Hauri, *Opt. Express* **19**, 20128 (2011)
- T. Oksenhendler, D. Kaplan, P. Tournois, G.M. Greetham, F. Estable, *Appl. Phys. B* **83**, 491 (2006)
- V. Petrov, *Opt. Mater.* **34**, 536 (2012)
- L. Isaenko, A. Yelisseyev, S. Lobanov, P. Krinitsin, V. Petrov, J.-J. Zondy, *J. Non. Cryst. Solids* **352**, 2439 (2006)
- G. Cerullo, S. De Silvestri, *Rev. Sci. Instrum.* **74**, 1 (2003)
- G. Arisholm, *J. Opt. Soc. Am. B* **14**, 2543 (1997)
- A. Dubietis, G. Jonušauskas, A. Piskarskas, *Opt. Commun.* **88**, 437 (1992)
- P. Schlup, J. Biegert, C.P. Hauri, G. Arisholm, U. Keller, *Appl. Phys. B* **79**, 285 (2004)
- C. Erny, L. Gallmann, U. Keller, *Appl. Phys. B* **96**, 257 (2009)
- R.Y. Chiao, P.L. Kelley, E. Garmire, *Phys. Rev. Lett.* **17**, 1158 (1966)
- H.K. Tsang, C.S. Wong, T.K. Liang, I.E. Day, S.W. Roberts, A. Harpin, J. Drake, M. Asghari, *Appl. Phys. Lett.* **80**, 416 (2002)
- S. Pearl, S. Fastig, Y. Ehrlich, R. Lavi, *Appl. Opt.* **40**, 2490 (2001)
- S. Marzenell, R. Beigang, R. Wallenstein, *Appl. Phys. B* **69**, 423 (1999)
- K.L. Vodopyanov, S.B. Mirov, V.G. Voevodin, P.G. Schunemann, *Opt. Commun.* **155**, 47 (1998)
- C. Wen-Dan, X. Zhi, W. Dong-Sheng, H. Shu-Ping, W. Jin-Yun, Z. Hao, *Chin. J. Struct. Chem.* **29**, 950 (2010)
- V. Petrov, A. Yelisseyev, L. Isaenko, S. Lobanov, A. Titov, J.-J. Zondy, *Appl. Phys. B* **78**, 543 (2004)
- K.L. Vodopyanov, L.A. Kulevskii, V.G. Voevodin, A.I. Gribenyukov, K.R. Allakhverdiev, T.A. Kerimov, *Opt. Commun.* **83**, 322 (1991)
- R.S. Feigelson, R.K. Route, *Opt. Eng.* **26**, 262113 (1987)
- L. Isaenko, A. Yelisseyev, S. Lobanov, V. Petrov, F. Rotermund, G. Slekyš, J.-J. Zondy, *J. Appl. Phys.* **91**, 9475 (2002)
- L. Isaenko, A. Yelisseyev, S. Lobanov, A. Titov, V. Petrov, J.-J. Zondy, P. Krinitsin, A. Merkulov, V. Vedenyapin, J. Smirnova, *Cryst. Res. Technol.* **38**, 379 (2003)
- A.O. Okorogu, S.B. Mirov, W. Lee, D.I. Crouthamel, N. Jenkins, A.Y. Dergachev, K.L. Vodopyanov, V.V. Badikov, *Opt. Commun.* **155**, 307 (1998)
- P. Canarelli, Z. Benko, R. Curl, F.K. Tittel, *J. Opt. Soc. Am. B* **9**, 197 (1992)